Optimization of Current Carrying Multicables

Helmut Harbrecht, Florian Loos

Institute of Mathematics
University of Basel
Rheinsprung 21
CH - 4051 Basel
Switzerland

Preprint No. 2013-16
June, 2013

www.math.unibas.ch

Noname manuscript No.
(will be inserted by the editor)

Optimization of current carrying multicables

Helmut Harbrecht · Florian Loos

Received: date / Accepted: date

Abstract High currents in cable bundles contribute to hotspot generation and overheating of essential car elements, especially in connecting structures. An important aspect in this context is the influence of the positioning of wires in cable harnesses. In order to find an appropriate multicable layout with minimized maximum temperatures, we formulate a corresponding optimization problem. Depending on the packing density of the cable bundle, it is solved via different optimization strategies: in case of loosely packed cable bundles solely by a gradient-based strategy (shape optimization), densely packed ones by arrangement heuristics combined with a standard genetic algorithm, others by mixed strategies.

In the simulation model, temperature dependence of the electric conductor resistances and different parameter values for the multitude of subdomains are respected in the governing semilinear and piecewise defined equation. Convective and radiative effects are summarized by a heat transfer coefficient in a nonlinear boundary condition at the exterior multicable surface. Finite elements in combination with an interior-point method and a genetic algorithm allow the solution of the optimization problem for a large number of cable bundle types. Furthermore, we present an adjoint method for the solution of the shape optimization problem. The jumps at the interfaces of different materials are essential for the Hadamard representation of the shape gradient. Numeri-

This research has been supported in parts by the German National Science Foundation (DFG) through the Priority Program 1253 "Optimierung mit partiellen Differentialgleichungen" (Optimization with partial differential equations).

H. Harbrecht
Mathematisches Institut, Universität Basel, Rheinsprung 21, 4051 Basel, Switzerland
E-mail: helmut.harbrecht@unibas.ch

F. Loos
Institut für Mathematik und Bauinformatik, Universität der Bundeswehr München, 85577 Neubiberg, Germany
E-mail: florian.loos@unibw.de

cal experiments are carried out to demonstrate the feasibility and scope of the present approach.

Keywords Shape optimization · Genetic algorithm · Electric cables · Finite element method · Joule heating

Mathematics Subject Classification (2000) 49Q10 · 49J20 · 65K10

1 Introduction

The number of electric devices in modern cars grows continuously whereas available space remains the same or even reduces. Especially in hybrid and electric cars, many components have to be supplied by high currents. To save material, space and weight, manufacturers reduce cable diameters which is only possible to a certain extend. Smaller diameters result in higher temperatures in the connecting structures. This could entail overheating and irreparable damages in essential components.

In [11], the modeling and simulation of heat transfer in current carrying multicables is described. Furthermore, the dependence of the heat distribution in the multicable on the composition and configuration of the single cables is shown by numerical experiments and measurements. Fig. 1 illustrates two different multicables, consisting of 33 single cables with same current and cross sectional area for each single cable in both cases. Furthermore, the multicable diameters, ambient temperatures and all other parameters are equal. Both only differ in the positioning of the single cables in the multicable. Obviously, the maximum temperature for the left single cable design is with 98.8 °C lower than for the right one with 107.4 °C.

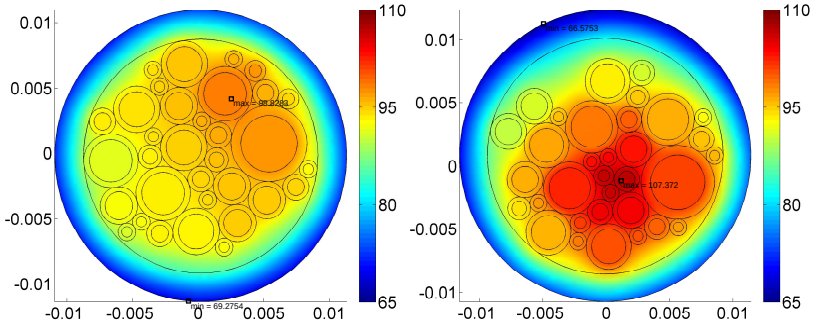

(a) Cable layout 1. (b) Cable layout 2.

Fig. 1: Comparison of temperature distributions for equally composed multicables varying in single cable positions.

In this paper, an algorithm to find an optimal multicable layout is developed. For each single cable, the current and the diameters are fixed a priori. Dependent on the number of single cables and available space, different strategies are recommended. Whereas for rather loosely packed cables the exclusive application of gradient-based shape optimization is sufficient, we additionally have to couple it to a genetic algorithm for dense cables. For the shape optimization part, we point out the derivation of an optimality system via the formal Lagrangian approach including an adjoint system and the shape gradient as well as the local shape derivative. In addition, we present our genetic algorithm adapted to the problem.

The simulation of temperature distribution in cable bundles and its computation is subject of several articles, e. g. [3,4,11,19]. In [2], algorithms for minimization of the total weight of cable bundles by given maximum temperature were developed. Therein, parallel multilevel methods are applied to heuristic strategies based on greedy type search methods. Our optimization problem is related. In contrast, we couple a non-gradient based strategy, namely a genetic algorithm, to a gradient-based shape optimization approach. For introductions to the shape calculus and mathematical background, we recommend [6,23,28]. Like in [20], we derive optimality conditions formally via the Langrange technique (cf. [29]). The particularity in the Hadamard representation of our shape gradient is due to the jumps in the coefficients of different materials at the interfaces. In [12,13,15], methods to derive the corresponding shape gradient are explained.

The paper is organized as follows: In section 2, we introduce our modeling and simulation approach to describe the heating of multicables. Besides the state system, we formulate the corresponding optimal multicable layout problem. Our general optimization strategy by combining a squeezing algorithm, heuristics for good initial positions, shape optimization and a genetic algorithm is explained in section 3. In order to obtain an optimality system, we apply the formal Lagrangian approach and use the local shape derivative in section 4. Apart from the adjoint system, the shape gradient is derived. Section 5 describes further numerical and computational details. Numerical experiments are carried out in section 6 and finally, we draw a conclusion and give an outlook to future work in section 7.

2 Setting of the problem

In this section, we introduce the mathematical notation, governing equations and formulate the optimal multicable layout problem.

2.1 Notation

We collect definitions and notations necessary for the mathematical description of our problem. Throughout this paper, we restrict ourselves to the stationary, two dimensional case. All vector valued functions are indicated by

bold letters, for example the space variable $\mathbf{x} = (x, y)^T \in \mathbb{R}^2$ with norm $|\mathbf{x}|_{\mathbb{R}^2} = \left(x^2 + y^2\right)^{1/2}$ and inner product $(\mathbf{x}_1, \mathbf{x}_2)$. The temperature in the domain $\Omega \subset \mathbb{R}^2$ is dependent on the position $\mathbf{x}$ and denoted by $T = T(\mathbf{x})$. We abbreviate its gradient by $\nabla T = \left(\frac{\partial T}{\partial x}, \frac{\partial T}{\partial y}\right)^T$ and the divergence operator by $\nabla\cdot = \left((\frac{\partial}{\partial x}, \frac{\partial}{\partial y})^T, \cdot\right)$. Div denotes the tangential divergence of a tangential field and ∇_τ the tangential (surface) gradient of a scalar valued function.

$\mathbf{n} = \mathbf{n}_\mathrm{e}$ represents the unit outer normal that points away from the surface of the considered object, $\mathbf{n}_\mathrm{i}$ the inner normal pointing into the object. Consequently, $\frac{\partial}{\partial \mathbf{n}}$ corresponds to the normal derivative of a quantity in outer direction. The notation $[\cdot]_\pm$ abbreviates the difference of the traces of a function at an interface boundary, approaching the boundary from exterior and interior respectively.

The k-th single cable $C_k = \left(x_k, y_k, r_k^\mathrm{in}, r_k^\mathrm{ex}\right)$ is geometrically described by its centre coordinates (x_k, y_k), the radius of the current carrying part r_k^in and the outer radius r_k^ex. The multicable $MC = \left(\left(x_0, y_0, r_0^\mathrm{in}, r_0^\mathrm{ex}\right); c_1, \ldots, c_N\right)$ consists of N single cables (cf. Fig. 2a for $N = 3$), has the centre coordinates (x_0, y_0) and the inner radius r_0^in respectively the outer radius r_0^ex. It is surrounded by an insulation layer of thickness $r_0^\mathrm{ex} - r_0^\mathrm{in}$ with heat conductivity λ^ex. Each single cable consists of a core part Ω_k^core with heat conductivity λ_k^core, carrying the current I_k, and an insulation part Ω_k^iso with heat conductivity λ_k^iso. The gaps between the single cables and the exterior insulation can be of solid material or air. Herein, they are modelled by pure conduction with heat conductivity λ^gaps.

The interfaces between core and insulation part of each single cable and between single cable insulation and surrounding gaps play an important role in the calculation of the shape gradient. Thus, we introduce the interface boundaries Γ_k^i and Γ_k^e for $k = 1, \ldots, N$. Furthermore, corresponding normal vectors on the boundaries are depicted in Fig. 2b:

2.2 State system

Let the two dimensional cross sectional area of the multicable Ω be a connected bounded domain in $\mathbb{R}^2$ with regular exterior boundary $\partial\Omega = \Gamma^\mathrm{ex}$ and interface boundaries $\Gamma^\mathrm{int} = \bigcup_{k=1}^N \left(\Gamma_k^\mathrm{i} \cup \Gamma_k^\mathrm{e}\right) \cup \Gamma^\mathrm{gi}$. Γ^gi represents the interface between the exterior insulation and the gaps. We suppose the cable to be entirely surrounded by air. Then, the temperature distribution $T(\mathbf{x})$ can be described by the following state system (cf. [11]):

$$\begin{aligned} -\nabla \cdot (\lambda \nabla T) - c \cdot T &= f \quad \text{in } \Omega, \\ \lambda^\mathrm{ex} \frac{\partial T}{\partial \mathbf{n}} + \alpha(T) \cdot \left(T - T^\mathrm{amb}\right) &= 0 \quad \text{on } \Gamma^\mathrm{ex} \end{aligned} \tag{1}$$

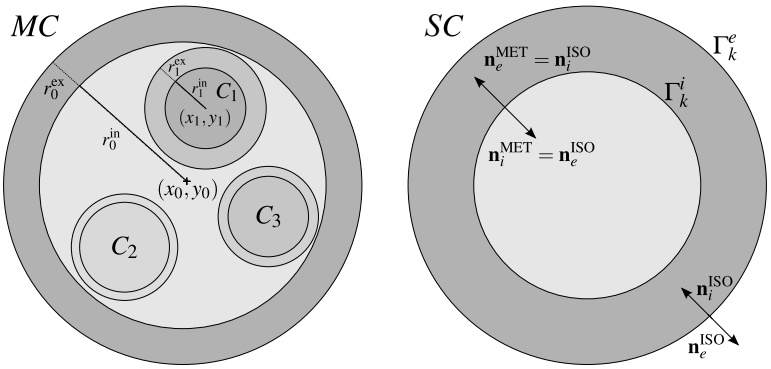

(a) (b)

Fig. 2: Model of (a) a multicable with three single cables and (b) the k-th single cable with corresponding geometrical quantities.

with

$$\lambda := \sum_{k=1}^{N} \left(\lambda_k^{\mathrm{core}} \, \mathbb{I}_{\Omega_k^{\mathrm{core}}} + \lambda_k^{\mathrm{iso}} \, \mathbb{I}_{\Omega_k^{\mathrm{iso}}} \right) + \lambda^{\mathrm{ex}} \, \mathbb{I}_{\Omega^{\mathrm{ex}}} + \lambda^{\mathrm{gaps}} \, \mathbb{I}_{\Omega^{\mathrm{gaps}}},$$

$$c := \sum_{k=1}^{N} \frac{1}{n_k} \left(\frac{4 I_k}{d_k^{\mathrm{in}} \delta_k \pi} \right)^2 \rho_{0,k} \, \alpha_{\rho,k} \, \mathbb{I}_{\Omega_k^{\mathrm{core}}},$$

$$f := \sum_{k=1}^{N} \frac{1}{n_k} \left(\frac{4 I_k}{d_k^{\mathrm{in}} \delta_k \pi} \right)^2 \rho_{0,k} \, (1 - \alpha_{\rho,k} \, T_{\mathrm{ref}}) \, \mathbb{I}_{\Omega_k^{\mathrm{core}}}.$$

Herein, λ denotes the heat conductivity, c the linear temperature coefficient and f the source term. All vary for the different subdomains, expressed by the indicator function $\mathbb{I}$. Furthermore, $\alpha(T)$ summarizes the heat transfer coefficient at Γ^{ex}, the transition of the exterior insulation material of the multicable to ambient air with temperature T^{amb}. It includes the effects of radiation and convection. The radiation is governed by the Stefan-Boltzmann law [18], convection is approximated by nonlinear formulas, obtained by fitting of empirical data [1,19]. For the identification of the further quantities, we refer to [11].

Due to the jumps of the heat conductivity, the temperature profile is continuous across the interface of different materials $\gamma \in \Gamma^{\mathrm{int}}$, but has kinks. Although an explicit mentioning of these conditions is not necessary for a concise problem presentation, we explicitly indicate them in the following reformulation of (1) as an interface problem which is important for the Hadamard presentation of the shape gradient:

$$\begin{aligned} -\nabla\cdot(\lambda\,\nabla T) - c\cdot T &= f && \text{in } \Omega\setminus\Gamma^{\mathrm{int}},\\ \lambda^{\mathrm{ex}}\,\frac{\partial T}{\partial \mathbf{n}} + \alpha(T)\cdot\left(T - T^{\mathrm{amb}}\right) &= 0 && \text{on } \Gamma^{\mathrm{ex}},\\ [T]_{\pm} = 0 \quad\text{and}\quad \left[\lambda\frac{\partial T}{\partial \mathbf{n}}\right]_{\pm} &= 0 && \text{on } \gamma\in\Gamma^{\mathrm{int}}. \end{aligned} \tag{2}$$

Note finally that the governing equation of (1) and (2), respectively, is the Helmholtz equation. In the given form, it has in general no unique solution and oscillations can exist, especially for higher values of c. [10,11] give conditions for which the solution is still unique. It is proved that in the present application, the values of c are small enough to provide a unique solution.

2.3 Optimization problem

Let the dimensions of the exterior insulation and the single cables be given. The material parameters and the currents for each single cable are fixed and known such that λ, c and f are determined a priori. What we vary is the inner form of the domain Ω by the positioning of the single cable. Thus, our optimization variables are the centre coordinates of the single cables $(x_1,y_1),\dots,(x_N,y_N)$. Consequently, the optimal mutlicable layout problem (OptMC) with dependent domain $\Omega=\Omega\left((x_1,y_1),\dots,(x_N,y_N)\right)$ reads as follows:

$$\begin{aligned} J(\Omega) &= \int_{\Omega} j\left(\mathbf{x},T(\mathbf{x})\right)\,\mathrm{d}\mathbf{x} \to \min! \\ \text{with}\quad -\nabla\cdot(\lambda\,\nabla T) - c\cdot T &= f \quad \text{in } \Omega\setminus\Gamma^{\mathrm{int}},\\ \lambda^{\mathrm{ex}}\,\frac{\partial T}{\partial \mathbf{n}} + \alpha(T)\cdot\left(T - T^{\mathrm{amb}}\right) &= 0 \quad \text{on } \Gamma^{\mathrm{ex}},\\ [T]_{\pm} = 0 \quad\text{and}\quad \left[\lambda\frac{\partial T}{\partial \mathbf{n}}\right]_{\pm} &= 0 \quad \text{on } \gamma\in\Gamma^{\mathrm{int}},\\ \text{s.t. } (x_k-x_0)^2+(y_k-y_0)^2 &\le \left(r_k^{\mathrm{ex}}-r_0^{\mathrm{in}}\right)^2, \qquad k\in K=\{1,\dots,N\},\\ (x_k-x_l)^2+(y_k-y_l)^2 &\ge \left(r_k^{\mathrm{ex}}+r_l^{\mathrm{ex}}\right)^2, \quad (k,l)\in(K\times K)\setminus\{k=l\},\\ x_1 = 0, \qquad 0\le y_1 &\le r_0^{\mathrm{in}}, \qquad 0\le x_2\le r_0^{\mathrm{in}}, \end{aligned} \tag{3}$$

It is the objective to minimize the cost functional $J(\Omega)$ respectively the function $j\left(\mathbf{x},T(\mathbf{x})\right)$ over the domain Ω subject to the state system (2) and geometrical constraints. We require that each single cable has to be entirely inside the multicable and single cables must not overlap.[1] As this problem is completely rotational symmetrical because the formula at the exterior boundary is everywhere equal, we allow the first cable to be positioned on the vertical

[1] To avoid problems in the calculation with finite elements, we require in the numerical implementation that the distance between each single cable and multicable insulation respectively pairwise between two single cables has to be larger than $\delta>0$. The parameter δ is chosen such that the space in between is sufficiently large to create a feasible mesh.

upper line segment connecting multicable centre and $(0, r_0^{\text{in}})$ solely. To avoid axial symmetry, the second cable has to be in the right half of the multicable. We summarize the set of admissible domains by

$$\begin{aligned}\mathcal{O}_{\text{ad}} = \big\{ \Omega = \Omega\left((x_1, y_1), \ldots, (x_N, y_N)\right) \in \mathbb{R}^2 \,|\, \\ (x_k - x_0)^2 + (y_k - y_0)^2 \leq \left(r_k^{\text{ex}} - r_0^{\text{in}}\right)^2,\ k \in K = \{1, \ldots, N\}, \\ (x_k - x_l)^2 + (y_k - y_l)^2 \geq (r_k^{\text{ex}} + r_l^{\text{ex}})^2,\ (k,l) \in (K \times K) \setminus \{k = l\}, \\ x_1 = 0,\ 0 \leq y_1 \leq r_0^{\text{in}},\ 0 \leq x_2 \leq r_0^{\text{in}} \big\}.\end{aligned}$$

3 Optimization

Dependent on the number of single cables in the multicable and the available space, different optimization strategies have to be applied. In this section, we describe our general optimization strategy, how to find good positions, the application of shape optimization and the genetic algorithm.

3.1 Optimization strategy

To solve the optimal multicable layout problem (3), we combine different algorithms and optimization techniques as shown in Fig. 3. To approximate a global minimum, we use M different initial positions, obtained by heuristics and the application of a cable squeezing algorithm [11]. Details are described in subsection 3.2.

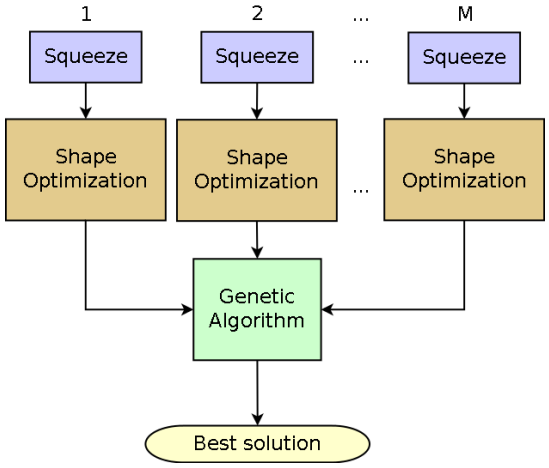

Fig. 3: Optimization strategy to solve the optimal multicable layout problem.

Using a gradient based strategy like shape optimization (cf. subsection 3.3) does not always provide a satisfying solution, as for multicables consisting of a large number of single cables several local minima exist. For that reason, we give our M local minima to a genetic algorithm (cf. subsection 3.4) which tries to find a better solution that corresponds to or at least approximates the global minimum. The coupling of these different algorithms is adequate as an exclusive use of the genetic algorithm is too time extensive and expensive. Furthermore, we obtain much better results in our simulations with the mixed strategies.

3.2 Initialization

As mentioned, different local minima can exist for more than three single cables. In order to ensure feasibility of the cable configurations, we apply the cable squeezing algorithm in [11]. It simulates the cable production process where each single cable is assigned to a template position and afterwards all cables are pressed together. After a fixed number of squeezing steps, the diameter of the surrounding circle including all single cable circles has to be smaller than or equal to the given inner diameter of the exterior insulation. If it is not the case, this initial template configuration can not be used for the optimization.

The initial cable configuration has an important influence on the computed local minimum and is mainly determined by the initial template assignment. Thus, we propose different heuristic strategies, dependent on the current over cross sectional area $J_k = I_k/A_k$, $k = 1, \ldots, n$, with A_k being the cross sectional area of the metallic part, to create good assignments of the single cables to their template positions:

- The single cables are assigned to the template positions in descending order dependent on J_k, denoted by INL;
- The single cables are assigned to the template positions in ascending order dependent on J_k, denoted by OUL;
- The single cables are ordered ascendantly but assigned to the template positions in steps of 2, 3, 4 respectively 5, denoted by OUL2, OUL3, OUL4 and OUL5;
- The single cables are assigned to template positions such that two cables following each other in order dependent on J_k have the greatest possible distance in the template layer, denoted by OPP;
- Further template configurations are completely arbitrary and denoted by MC1, MC2, ...

By tendency, hotter single cables can give more thermal energy to the ambience if they are nearer to the exterior border. For that, especially OUL, OUL2–OUL5 and OPP are promising to give good configurations, but need not necessarily. As there exist cases where other template configurations yield our best solution, we added INL and the arbitrary assignments.

3.3 Shape optimization

A general shape optimization problem looks as follows:

$$J(\Omega) = \int_{\Omega} j_1\big(\mathbf{x}, u(\mathbf{x}), \nabla u(\mathbf{x})\big)\,\mathrm{d}\mathbf{x} + \int_{\Gamma} j_2\big(\mathbf{x}, u(\mathbf{x}), \nabla u(\mathbf{x})\big)\,\mathrm{d}\sigma \to \min_{\Omega\in\mathcal{O}_{\mathrm{ad}}} !$$

subject to

$$\mathcal{A}u = f \text{ in } \Omega, \quad \mathcal{B}u = g \text{ on } \Gamma.$$

Here, J represents the function to be optimized, dependent on the domain Ω which is contained in the set of admissible domains $\mathcal{O}_{\mathrm{ad}}$. The function $u : \Omega \to \mathbb{R}$ is the solution to the partial differential equation with the second order differential operator $\mathcal{A}$ and the boundary condition described by the operator $\mathcal{B}$. The functions $j_1, j_2 : D\times\mathbb{R}\times\mathbb{R}^n \to \mathbb{R}$, $f, g : D \to \mathbb{R}$ are sufficiently smooth where the set $D \subseteq \mathbb{R}^n$ is the hold all which is assumed to always contain the (varying) domain Ω. For a general overview on shape calculus, we refer the reader e. g. to [6,23,28].

In order to compute the derivative of a function with respect to the geometry, we apply the *perturbation of identity* [22]. A bounded reference domain Ω_{ref} is fixed and $\Omega \in \mathcal{O}_{\mathrm{ad}}$ correspond to transformations of Ω_{ref}.

For a smooth perturbation field $\mathbf{V} : D \to \mathbb{R}^n$, we consider the perturbed domain

$$\Omega_\epsilon[\mathbf{V}] := \{\mathbf{x} + \epsilon\mathbf{V}(\mathbf{x}) : \mathbf{x} \in \Omega\}$$

with $\epsilon > 0$ sufficiently small [22], see Fig. 4 for an illustration. This enables the definition of the *shape derivative* of the shape functional J at Ω in direction of a vector field $\mathbf{V}$ by

$$\delta J(\Omega)[\mathbf{V}] := \lim_{\epsilon\to 0} \frac{J(\Omega_\epsilon[\mathbf{V}]) - J(\Omega)}{\epsilon}. \tag{4}$$

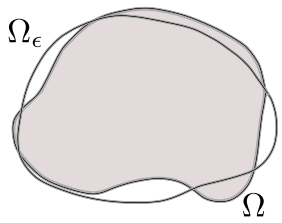

Fig. 4: The domain Ω and its perturbation Ω_ϵ.

The shape functional J is shape differentiable at Ω if the Eulerian derivative $\delta J(\Omega)[\mathbf{V}]$ exists for all directions $\mathbf{V}$ and the mapping $\mathbf{V} \mapsto \delta J(\Omega)[\mathbf{V}]$

is linear and continuous. To compute the shape derivative efficiently, we state the so-called Hadamard formula [27,28]:

Theorem 1 *Let J be shape differentiable according to (4). Then, the relation*

$$\delta J(\Omega)[\mathbf{V}] = \delta J(\Gamma)\,[\langle \mathbf{V}, \mathbf{n}\rangle\,\mathbf{n}]$$

holds for all vector fields $\mathbf{V} \in C^k(\bar{D}; \mathbb{R}^d)$ with $k \geq 1$ appropriately chosen.

Furthermore, we shall introduce the local shape derivative $\delta u = \delta u[\mathbf{V}]$ that describes the sensitivity of the PDE solution concerning domain variations. It is pointwisely defined by

$$\delta u(\mathbf{x}) := \lim_{\epsilon \to 0} \frac{u_\epsilon(\mathbf{x}) - u(\mathbf{x})}{\epsilon}, \quad \mathbf{x} \in \Omega \cap \Omega_\epsilon,$$

where u_ϵ denotes the solution of the boundary value problem on the perturbed domain.

The local shape derivative $\delta u = \delta u[\mathbf{V}]$ and the shape gradient $\delta J(\Omega)\,[\mathbf{V}]$ are essential for the sensitivity analysis of the problem in section 4.

3.4 Genetic algorithm

We describe how a genetic algorithm works based on [14,21]. A genetic algorithm is a stochastic method that can be used to solve optimization problems, e. g. to find a function's minimum, however not as precisely as gradient based methods or equivalent, for this method does not study the function to minimize. It only evaluates the function for a given number of optimization variable values (individuals).

The algorithm uses the concept of natural evolution (see Fig. 5): an initial population of individuals evolves in several generations using the simulated genetic operations *crossover* and *mutation*, letting the fittest individuals survive and reproduce. The initial population is made up of the M individuals obtained via the specified heuristics and can be completed by random individuals.

Let us apply this concept to our problem: each individual represents a set of possible coordinates for the single cables and we evaluate the fitness of each (value of the objective function for the cable configuration) in order to determine which individuals are the 'better' ones. To simulate the transition from a generation to the next one, we use the following steps:

- The reproduction is subject to the fitness: the k best individuals are directly transmitted to the next generation as *elite* and the parents are stochastically selected in the rest of the population.
- The coordinates of the parents are *crossed* and *mutated* to produce the 'children'.
- The new population of coordinates replaces the old one.

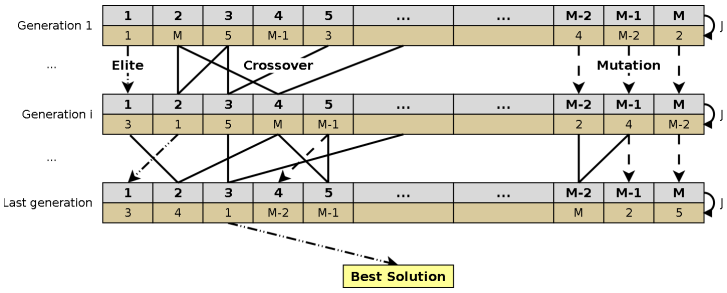

Fig. 5: Diagram of the genetic algorithm.

In our algorithm, the genetic algorithm proposes a cable configuration (by crossover or mutation). To make it feasible and locally optimal, we apply squeezing and shape optimization. This (locally) optimal value corresponds to the fitness value of the individual.

3.4.1 Crossover

Crossover children are created by combining the vectors of a pair of parents: we randomly select components from both parents and create the child with these components. For example, for two parents p_1, p_2 and one child c, the result could look like this:

$$\begin{aligned} p_1 &= [1, 2, 3, 4, 5, 6, 7] \\ p_2 &= [a, b, c, d, e, f, g] \\ c &= [1, 2, c, 4, e, f, 7]. \end{aligned}$$

3.4.2 Mutation

Mutation children are created by randomly modifying a certain number of components of the parent. In our case, we pick some components of the parent and take the average of these components with a random number r_i. For example, a mutation could look like this:

$$\begin{aligned} p &= [a, b, c, d, e, f, g] \\ c &= \left[a, \frac{b + r_1}{2}, c, d, \frac{e + r_2}{2}, \frac{f + r_3}{2}, g\right]. \end{aligned}$$

Each created individual (by crossover or mutation) has to be tested to ensure it respects the constraints of the problem. If however it does not, we apply the squeezing algorithm on it until it respects the given criteria, and if the squeezing algorithms fails, the non-conform individual is erased and newly created.

3.4.3 Stopping criterion

As there is no natural stopping criterion for this algorithm, we choose to stop it either after a certain number of generations or if there is no improvement in the fitness of the best individual in the population for several steps.

4 Sensitivity analysis

To derive an optimality system for (3), we apply the formal Lagrangian technique [20,29]. By taking corresponding variations to zero, one obtains an adjoint system and the necessary condition for a stationary point, namely the shape gradient to be equal to zero. In the following, we suppose the underlying functions to be sufficiently smooth to ensure well-posedness of all operations.

4.1 Formal Lagrange approach

We define the Lagrange function $\mathcal{L}$ for (3) by subtracting integrals over the equation on the domain and the exterior boundary from the objective function $J(\Omega, T(\Omega))$. As mentioned, the interface conditions are not necessary for a concise problem formulation. Consequently, they and also the geometrical constraints are not considered in the Lagrange function. Denoting the Lagrange multipliers by p_1, p_2, we thus have

$$\begin{aligned}\mathcal{L}(T,\Omega,p_1,p_2) = J(\Omega) &- \int_\Omega (\nabla\cdot(\lambda\,\nabla T) + cT + f)\,p_1\,\mathrm{d}\mathbf{x}\\ &- \int_{\Gamma^{\mathrm{ex}}} \left(\lambda^{\mathrm{ex}}\frac{\partial T}{\partial \mathbf{n}} + \alpha(T)\left(T - T^{\mathrm{amb}}\right)\right) p_2\,\mathrm{d}\sigma.\end{aligned}$$

Dividing Ω in subdomains and applying Green's formula on each subdomain leads, in view of the given jump conditions at the interfaces, to

$$\begin{aligned}&\mathcal{L}(T,\Omega,p_1,p_2)\\ &= J(\Omega) - \int_\Omega (\nabla\cdot(\lambda\,\nabla p_1) + c\,p_1)\,T\,\mathrm{d}\mathbf{x} - \int_\Omega f\,p_1\,\mathrm{d}\mathbf{x} - \int_{\Gamma^{\mathrm{ex}}} \lambda^{\mathrm{ex}}\frac{\partial T}{\partial \mathbf{n}} p_2\,\mathrm{d}\sigma\\ &- \int_{\Gamma^{\mathrm{ex}}} \alpha(T)\left(T - T^{\mathrm{amb}}\right) p_2\,\mathrm{d}\sigma - \int_{\Gamma^{\mathrm{ex}}} \lambda^{\mathrm{ex}}\frac{\partial T}{\partial \mathbf{n}} p_1\,\mathrm{d}\sigma + \int_{\Gamma^{\mathrm{ex}}} \lambda^{\mathrm{ex}}\frac{\partial p_1}{\partial \mathbf{n}} T\,\mathrm{d}\sigma\\ &- \sum_{\gamma\in\Gamma^{\mathrm{int}}}\left[\int_\gamma \lambda^{\mathrm{e}}\frac{\partial T^{\mathrm{e}}}{\partial \mathbf{n}}\left(p_1^{\mathrm{e}} - p_1^{\mathrm{i}}\right)\,\mathrm{d}\sigma - \int_\gamma T^{\mathrm{e}}\left(\lambda^{\mathrm{e}}\frac{\partial p_1^{\mathrm{e}}}{\partial \mathbf{n}} - \lambda^{\mathrm{i}}\frac{\partial p_1^{\mathrm{i}}}{\partial \mathbf{n}}\right)\,\mathrm{d}\sigma\right].\end{aligned}$$

In this expression, taking the outer trace at the interior interface $\gamma \in \Gamma^{\mathrm{int}}$ is indicated by the suffix $\cdot^{\mathrm{e}}$, whereas taking the inner trace at the interior interface $\gamma \in \Gamma^{\mathrm{int}}$ is indicated by the suffix $\cdot^{\mathrm{i}}$.

Let $\left(\bar{T}, \bar{\Omega}\right)$ be an optimal pair of (3). Then, the first variations of $\mathcal{L}$ with respect to p_1, p_2, T and Ω in the directions h_{p_1}, h_{p_2}, h_T and h_Ω are all zero, i. e., the following first order optimality conditions hold:

$$\begin{aligned} \mathcal{L}_{p_1}\left(\bar{T}, \bar{\Omega}, p_1, p_2\right) h_{p_1} &= 0, \\ \mathcal{L}_{p_2}\left(\bar{T}, \bar{\Omega}, p_1, p_2\right) h_{p_2} &= 0, \\ \mathcal{L}_{T}\left(\bar{T}, \bar{\Omega}, p_1, p_2\right) h_{T} &= 0, \\ \mathcal{L}_{\Omega}\left(\bar{T}, \bar{\Omega}, p_1, p_2\right) h_{\Omega} &= 0. \end{aligned} \tag{5}$$

The variation of $\mathcal{L}$ with respect to the Lagrange multipliers yields the state system (2), the variation with respect to the temperature provides the adjoint system and, by the variation with respect to the domain, we obtain the necessary optimality condition for stationary points, see [20].

4.2 Adjoint system

Taking the first variation of $\mathcal{L}$ with respect to the temperature T in the direction $h_T \in H^1(\Omega)$ to zero provides the identity

$$\begin{aligned} 0 &= \mathcal{L}_T\left(\bar{T}, \bar{\Omega}, p_1, p_2\right) h_T \\ &= \int_\Omega \frac{\partial j}{\partial T}(\mathbf{x}, \bar{T}) h_T \,\mathrm{d}\mathbf{x} - \int_\Omega \left(\nabla \cdot (\lambda \nabla p_1) + c\, p_1\right) h_T \,\mathrm{d}\mathbf{x} \\ &\quad - \int_{\Gamma^{\mathrm{ex}}} \lambda^{\mathrm{ex}} \frac{\partial h_T}{\partial \mathbf{n}} p_2 \,\mathrm{d}\sigma - \int_{\Gamma^{\mathrm{ex}}} \left(\alpha'(\bar{T})\left(\bar{T} - T^{\mathrm{amb}}\right) + \alpha(\bar{T})\right) h_T\, p_2 \,\mathrm{d}\sigma \\ &\quad - \int_{\Gamma^{\mathrm{ex}}} \lambda^{\mathrm{ex}} \frac{\partial h_T}{\partial \mathbf{n}} p_1 \,\mathrm{d}\sigma + \int_{\Gamma^{\mathrm{ex}}} \lambda^{\mathrm{ex}} \frac{\partial p_1}{\partial \mathbf{n}} h_T \,\mathrm{d}\sigma \\ &\quad - \sum_{\gamma \in \Gamma^{\mathrm{int}}} \left[\int_\gamma \lambda^{\mathrm{e}} \frac{\partial h_T^{\mathrm{e}}}{\partial \mathbf{n}} \left(p_1^{\mathrm{e}} - p_1^{\mathrm{i}}\right) \,\mathrm{d}\sigma - \int_\gamma h_T^{\mathrm{e}} \left(\lambda^{\mathrm{e}} \frac{\partial p_1^{\mathrm{e}}}{\partial \mathbf{n}} - \lambda^{\mathrm{i}} \frac{\partial p_1^{\mathrm{i}}}{\partial \mathbf{n}}\right) \,\mathrm{d}\sigma \right]. \end{aligned}$$

If it holds $h_T \in C_0^\infty(\Omega)$ with $h_T = \frac{\partial h_T}{\partial \mathbf{n}} = 0$ on all $\gamma \in \Gamma^{\mathrm{int}}$, one obtains

$$\int_\Omega \frac{\partial j}{\partial T}(\mathbf{x}, \bar{T}) h_T \,\mathrm{d}\mathbf{x} = \int_\Omega \left(\nabla \cdot (\lambda \nabla p_1) + c\, p_1\right) h_T \,\mathrm{d}\mathbf{x},$$

which implies that p_1 satisfies the partial differential equation

$$\nabla \cdot (\lambda \nabla p_1) + c\, p_1 = \frac{\partial j}{\partial T}(\cdot, \bar{T}) \ \text{ in } \ \Omega \setminus \Gamma^{\mathrm{int}}. \tag{6}$$

To conclude the associate boundary conditions, we consider $h_T \in H_0^1(\Omega)$ such that $h_T = \frac{\partial h_T}{\partial \mathbf{n}} = 0$ on all $\gamma \in \Gamma^{\mathrm{int}}$ and $\frac{\partial h_T}{\partial \mathbf{n}}$ arbitrary on Γ^{ex}. This yields

$$-\int_{\Gamma^{\mathrm{ex}}} \lambda^{\mathrm{ex}} \frac{\partial h_T}{\partial \mathbf{n}} p_1 \,\mathrm{d}\sigma - \int_{\Gamma^{\mathrm{ex}}} \lambda^{\mathrm{ex}} \frac{\partial h_T}{\partial \mathbf{n}} p_2 \,\mathrm{d}\sigma = 0,$$

which means that $p_1 = -p_2$. We define $p := p_1 = -p_2$ and apply next an arbitrary $h_T \in H^1(\Omega)$ and $h_T = \frac{\partial h_T}{\partial \mathbf{n}} = 0$ on all $\gamma \in \Gamma^{\mathrm{int}}$ to provide

$$\int_{\Gamma^{\mathrm{ex}}} \lambda^{\mathrm{ex}} \frac{\partial p}{\partial \mathbf{n}} h_T \,\mathrm{d}\sigma + \int_{\Gamma^{\mathrm{ex}}} \left(\alpha'(\bar{T})\left(\bar{T} - T^{\mathrm{amb}}\right) + \alpha(\bar{T})\right) h_T \, p \,\mathrm{d}\sigma = 0.$$

Hence, we arrive at the Robin boundary condition

$$\lambda^{\mathrm{ex}} \frac{\partial p}{\partial \mathbf{n}} + \left(\alpha'(\bar{T})\left(\bar{T} - T^{\mathrm{amb}}\right) + \alpha(\bar{T})\right) p = 0 \ \text{ on } \ \Gamma^{\mathrm{ex}}. \tag{7}$$

Let $\gamma \in \Gamma^{\mathrm{int}}$ be an arbitrary, but fixed and connected interface boundary. By choosing $h_T \in H^1(\Omega)$ such that $h_T = 0$ on γ and $h_T = \frac{\partial h_T}{\partial \mathbf{n}} = 0$ on all $\tilde{\gamma} \in \Gamma^{\mathrm{int}} \setminus \gamma$, we get the Dirichlet jump condition

$$p^{\mathrm{e}} = p^{\mathrm{i}} \ \Leftrightarrow \ \left[p\right]_{\pm} = 0 \quad \text{on } \gamma \in \Gamma^{\mathrm{int}}. \tag{8}$$

Finally, for $\gamma \in \Gamma^{\mathrm{int}}$ arbitrary, fixed and connected, the choice $h_T \in H^1(\Omega)$ such that $h_T = \frac{\partial h_T}{\partial \mathbf{n}} = 0$ on all $\tilde{\gamma} \in \Gamma^{\mathrm{int}} \setminus \gamma$ gives the Neumann jump condition at the interface γ

$$\lambda^{\mathrm{e}} \frac{\partial p_1^{\mathrm{e}}}{\partial \mathbf{n}} = \lambda^{\mathrm{i}} \frac{\partial p_1^{\mathrm{i}}}{\partial \mathbf{n}} \ \Leftrightarrow \ \left[\lambda \frac{\partial p}{\partial \mathbf{n}}\right]_{\pm} = 0 \quad \text{on } \gamma \in \Gamma^{\mathrm{int}}. \tag{9}$$

As $\gamma \in \Gamma^{\mathrm{int}}$ arbitrary, the interface conditions (8) and (9) hold for all $\gamma \in \Gamma^{\mathrm{int}}$. Thus, combining (6)–(9), the adjoint p solves the following system and corresponds to $p = p_1 = -p_2$:

$$\begin{aligned} \nabla \cdot (\lambda \nabla p) + c \cdot p &= \frac{\partial j}{\partial T}(\cdot, T) \quad \text{in } \Omega \setminus \Gamma^{\mathrm{int}}, \\ \lambda^{\mathrm{ex}} \frac{\partial p}{\partial \mathbf{n}} + \left(\alpha'(T)\left(T - T^{\mathrm{amb}}\right) + \alpha(T)\right) p &= 0 \quad \text{on } \Gamma^{\mathrm{ex}}, \\ \left[p\right]_{\pm} = 0 \quad \text{and} \quad \left[\lambda \frac{\partial p}{\partial \mathbf{n}}\right]_{\pm} &= 0 \quad \text{on } \gamma \in \Gamma^{\mathrm{int}}. \end{aligned} \tag{10}$$

4.3 Local shape derivative

Before deriving the shape gradient and the necessary condition for a minimum of (3), we state the equations holding for the local shape derivative $\delta T[\mathbf{V}]$ of (OptMC). To this end, let $\mathbf{V}$ be a smooth domain variation of Ω which keeps the boundary Γ^{ex} fixed. Then, it holds

$$
\begin{aligned}
&\nabla \cdot (\lambda \nabla \delta T[\mathbf{V}]) + c \cdot \delta T[\mathbf{V}] = 0 \ \text{ in } \ \Omega \setminus \Gamma^{\mathrm{int}}, \\
&\lambda^{\mathrm{ex}} \frac{\partial \delta T\,[\mathbf{V}]}{\partial \mathbf{n}} + \left(\alpha'\,(T)\left(T - T^{\mathrm{amb}}\right) + \alpha(T)\right) \delta T\,[\mathbf{V}] = 0 \ \text{ on } \ \Gamma^{\mathrm{ex}}, \\
&\left[\lambda \frac{\partial \delta T\,[\mathbf{V}]}{\partial \mathbf{n}}\right]_{\pm} = \mathrm{Div}\left(\langle \mathbf{V}, \mathbf{n}\rangle\,[\lambda]_{\pm}\,\nabla_{\tau} T\right) + \left([c]_{\pm}\,T + [f]_{\pm}\right)\langle \mathbf{V}, \mathbf{n}\rangle \qquad (11) \\
&\text{and } \ \left[\delta T\,[\mathbf{V}]\right]_{\pm} = -\,\langle \mathbf{V}, \mathbf{n}\rangle \left[\frac{\partial T}{\partial \mathbf{n}}\right]_{\pm} \ \text{ on } \ \Gamma^{\mathrm{int}}.
\end{aligned}
$$

Proof The pointwise evaluation of the boundary value problem for T respectively $T_\epsilon[\mathbf{V}]$ on the domains Ω respectively $\Omega_\epsilon[\mathbf{V}]$ in a point $\mathbf{x} \in \Omega \cap \Omega_\epsilon[\mathbf{V}]$ provides

$$
\lim_{\epsilon \to 0} \frac{\nabla \cdot (\lambda \nabla T_\epsilon[\mathbf{V}]) + c \cdot T_\epsilon[\mathbf{V}] - (\nabla \cdot (\lambda \nabla T) + c \cdot T)}{\epsilon} = -f + f = 0,
$$

that is the partial differential equation

$$
\nabla \cdot (\lambda \nabla \delta T[\mathbf{V}]) + c \cdot \delta T[\mathbf{V}] = 0 \ \text{ in } \ \Omega \setminus \Gamma^{\mathrm{int}}.
$$

On the boundary condition on the exterior boundary, one obtains

$$
\lim_{\epsilon \to 0} \lambda^{\mathrm{ex}} \frac{\frac{\partial T_\epsilon[\mathbf{V}]}{\partial \mathbf{n}} - \frac{\partial T}{\partial \mathbf{n}}}{\epsilon} = -\lim_{\epsilon \to 0} \frac{\alpha(T_\epsilon[\mathbf{V}])(T_\epsilon[\mathbf{V}] - T^{\mathrm{amb}}) - \alpha(T)(T - T^{\mathrm{amb}})}{\epsilon}.
$$

Here, the term on the left hand side yields

$$
\lim_{\epsilon \to 0} \lambda^{\mathrm{ex}} \frac{\frac{\partial T_\epsilon[\mathbf{V}]}{\partial \mathbf{n}} - \frac{\partial T}{\partial \mathbf{n}}}{\epsilon} = \lambda^{\mathrm{ex}} \frac{\partial \delta T\,[\mathbf{V}]}{\partial \mathbf{n}},
$$

while the term on the right hand side provides

$$
\begin{aligned}
&\lim_{\epsilon \to 0} \frac{\alpha(T_\epsilon[\mathbf{V}])(T_\epsilon[\mathbf{V}] - T^{\mathrm{amb}}) - \alpha(T)(T - T^{\mathrm{amb}})}{\epsilon} \\
&= \lim_{\epsilon \to 0} \left(\frac{\alpha(T_\epsilon[\mathbf{V}]) - \alpha(T)}{\epsilon} \left(T_\epsilon[\mathbf{V}] - T^{\mathrm{amb}}\right) + \alpha(T) \frac{T_\epsilon[\mathbf{V}] - T}{\epsilon} \right) \\
&= \left(\alpha'\,(T)\left(T - T^{\mathrm{amb}}\right) + \alpha(T)\right) \delta T\,[\mathbf{V}]\,.
\end{aligned}
$$

Putting the latter two identities together yields the desired boundary conditions at Γ^{ex}.

Finally, for the interface conditions of the local shape derivative, we refer to [15,16].

4.4 Shape gradient

We reformulate (3) equivalently (see [20]) by

$$\min_{\Omega\in\mathcal{O}_{\mathrm{ad}},T}\Big\{\max_{p}\mathcal{L}(T,\Omega,p)\Big\}. \tag{12}$$

The theory of min-max problems [24] provides

$$\delta J(\Omega)\,[\mathbf{V}]=\mathcal{L}_{\Omega}\,(T,\Omega,p)\,h_{\Omega}\ \text{ with }\ \mathbf{V}=h_{\Omega}$$

at the solution of the min-max formulation (12). For an optimal interior point, the necessary optimality condition

$$\delta J(\Omega)\,[\mathbf{V}]=0$$

has to be fulfilled for all directions $\mathbf{V}$. The Hadamard representation of the shape gradient for (OptMC) reads as follows:

$$\begin{aligned}\delta J(\Omega)\,[\mathbf{V}]=\sum_{\gamma\in\Gamma^{\mathrm{int}}}\int_{\gamma}\langle\mathbf{V},\mathbf{n}\rangle\Big\{&\nabla_{\tau}p_{\mathrm{e}}\nabla_{\tau}T_{\mathrm{e}}[\lambda]_{\pm}\\&-p^{\mathrm{e}}\left([c]_{\pm}\,T^{\mathrm{e}}+[f]_{\pm}\right)-\lambda^{\mathrm{e}}\frac{\partial p^{\mathrm{e}}}{\partial\mathbf{n}}\left[\frac{\partial T}{\partial\mathbf{n}}\right]_{\pm}\Big\}\,\mathrm{d}\sigma.\end{aligned} \tag{13}$$

Proof Differentiation of $J(\Omega)$ in the direction $\mathbf{V}$ leads, in terms of the local shape derivative (11), to

$$\begin{aligned}\delta J(\Omega)\,[\mathbf{V}]=&\int_{\Omega}\frac{\partial j}{\partial T}\,(\mathbf{x},T)\cdot\delta T\,[\mathbf{V}]\,\mathrm{d}\mathbf{x}\\&+\sum_{\gamma\in\Gamma^{\mathrm{int}}}\int_{\gamma}\langle\mathbf{V},\mathbf{n}_{\mathrm{e}}\rangle\,j(\mathbf{x},T)+\langle\mathbf{V},\mathbf{n}_{\mathrm{i}}\rangle\,j(\mathbf{x},T)\,\mathrm{d}\sigma.\end{aligned}$$

With the adjoint system (10), we get

$$\begin{aligned}\delta J(\Omega)\,[\mathbf{V}]=&\int_{\Omega}(\nabla\cdot(\lambda\nabla p)+c\,p)\,\delta T\,[\mathbf{V}]\,\mathrm{d}\mathbf{x}\\&+\sum_{\gamma\in\Gamma^{\mathrm{int}}}\int_{\gamma}\langle\mathbf{V},\mathbf{n}_{\mathrm{e}}\rangle\,j(\mathbf{x},T)+\langle\mathbf{V},\mathbf{n}_{\mathrm{i}}\rangle\,j(\mathbf{x},T)\,\mathrm{d}\sigma.\end{aligned}$$

Application of Green's formula provides

$$\begin{aligned}
\delta J(\Omega)[\mathbf{V}] = &\int_{\Omega} \underbrace{\left(\nabla\cdot(\lambda\nabla\delta T[\mathbf{V}]) + c\cdot\delta T[\mathbf{V}]\right)p}_{=0}\,\mathrm{d}\mathbf{x} \\
&+ \int_{\Gamma^{\mathrm{ex}}} \underbrace{\left(\lambda^{\mathrm{ex}}\frac{\partial p}{\partial \mathbf{n}}\delta T[\mathbf{V}] - \lambda^{\mathrm{ex}}\frac{\partial \delta T[\mathbf{V}]}{\partial \mathbf{n}}p\right)}_{=0}\,\mathrm{d}\sigma \\
&+ \sum_{\gamma\in\Gamma^{\mathrm{int}}}\Bigg[\int_{\gamma}\left(\lambda^{\mathrm{i}}\frac{\partial p^{\mathrm{i}}}{\partial \mathbf{n}_{\mathrm{i}}}\delta T^{\mathrm{i}}[\mathbf{V}] - \lambda^{\mathrm{i}}\frac{\partial \delta T^{\mathrm{i}}[\mathbf{V}]}{\partial \mathbf{n}_{\mathrm{i}}}p^{\mathrm{i}}\right)\mathrm{d}\sigma \\
&\qquad + \int_{\gamma}\left(\lambda\frac{\partial p^{\mathrm{e}}}{\partial \mathbf{n}_{\mathrm{e}}}\delta T^{\mathrm{e}}[\mathbf{V}] - \lambda^{\mathrm{e}}\frac{\partial \delta T^{\mathrm{e}}[\mathbf{V}]}{\partial \mathbf{n}_{\mathrm{e}}}p^{\mathrm{e}}\right)\mathrm{d}\sigma\Bigg] \\
&= \sum_{\gamma\in\Gamma^{\mathrm{int}}}\left[\int_{\gamma}\lambda^{\mathrm{e}}\frac{\partial p^{\mathrm{e}}}{\partial \mathbf{n}}\left[\delta T[\mathbf{V}]\right]_{\pm}\mathrm{d}\sigma - \int_{\gamma}p^{\mathrm{e}}\left[\lambda\frac{\partial \delta T[\mathbf{V}]}{\partial \mathbf{n}}\right]_{\pm}\mathrm{d}\sigma\right].
\end{aligned}$$

Replacing the jumps in the Dirichlet data and the Neumann data by the interface conditions in (11) results in

$$\begin{aligned}
\delta J(\Omega)[\mathbf{V}] = &\sum_{\gamma\in\Gamma^{\mathrm{int}}}\int_{\gamma} -\lambda^{\mathrm{e}}\frac{\partial p^{\mathrm{e}}}{\partial \mathbf{n}}\langle\mathbf{V},\mathbf{n}\rangle\left[\frac{\partial T}{\partial \mathbf{n}}\right]_{\pm} \\
&- p^{\mathrm{e}}\Big(\mathrm{Div}\left(\langle\mathbf{V},\mathbf{n}\rangle[\lambda]_{\pm}\nabla_{\tau}T^{\mathrm{e}}\right) + \left([c]_{\pm}T^{\mathrm{e}} + [f]_{\pm}\right)\langle\mathbf{V},\mathbf{n}\rangle\Big)\,\mathrm{d}\sigma.
\end{aligned}$$

Integration by parts on the interface boundaries

$$-\int_{\gamma} p^{\mathrm{e}}\mathrm{Div}\left(\langle\mathbf{V},\mathbf{n}\rangle[\lambda]_{\pm}\nabla_{\tau}T^{\mathrm{e}}\right)\mathrm{d}\sigma = \int_{\gamma}\nabla_{\tau}p^{\mathrm{e}}\nabla_{\tau}T^{\mathrm{e}}\langle\mathbf{V},\mathbf{n}\rangle[\lambda]_{\pm}\,\mathrm{d}\sigma$$

finally implies the desired Hadamard representation of the shape gradient.

5 Algorithmic and numerical implementation

5.1 Shape functional

Aim of our calculations is to minimize the maximum temperature in a multicable. As the objective function

$$J(\Omega) = \min_{\Omega\in\mathcal{O}_{\mathrm{ad}}}\|T\|_{L^{\infty}(\Omega)} = \min_{\Omega\in\mathcal{O}_{\mathrm{ad}}}\int_{\Omega}\sup_{\bar{\mathbf{x}}\in\Omega}|T(\bar{\mathbf{x}})|\,\mathrm{d}\mathbf{x}$$

is not differentiable and thus the shape optimization approach would not be applicable, we approximate J by

$$J(\Omega) \approx \min_{\Omega \in \mathcal{O}_{\mathrm{ad}}} \frac{1}{q} \|T\|^q_{L^q(\Omega)} = \min_{\Omega \in \mathcal{O}_{\mathrm{ad}}} \frac{1}{q} \int_\Omega |T(\mathbf{x})|^q \, \mathrm{d}\mathbf{x}$$

for higher values of q. In (10), the derivative of the objective functional appears on the right hand side of the partial differential equation. As for too high values of q, the right hand side could explode and result in numerical problems, we use values of $q = 2, 3, 4$ or 5 in general.

5.2 Computation of jumps in Neumann data and gradient control

In order to ensure the correctness of the gradient implementation based on the adjoint method, we validate it by a non-adjoint method. To simplify notation, we introduce the reduced objective functional $\tilde{J}$, being explicitly dependent on $x_1, y_1, \ldots, x_N, y_N$:

$$\tilde{J}(x_1, y_1, \ldots, x_N, y_N) = J(\Omega(x_1, y_1, \ldots, x_N, y_N))$$

with the gradient

$$\nabla \tilde{J} = \left(\frac{\partial \tilde{J}}{\partial x_1}, \ldots, \frac{\partial \tilde{J}}{\partial y_N} \right)^T .$$

The partial derivative of $\tilde{J}$ to x_i is approximated via finite differences by

$$\frac{\partial \tilde{J}}{\partial x_i} \approx \lim_{\epsilon \to 0} \frac{\tilde{J}(\ldots, x_i + \epsilon, \ldots) - \tilde{J}(\ldots, x_i, \ldots)}{\epsilon}$$

where ϵ is a fixed and small value.

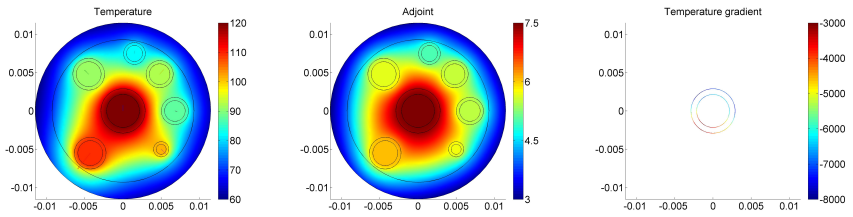

(a) (b) (c)

Fig. 6: (a) Temperature distribution in a multicable, (b) the associated adjoint solution on a multicable, and (c) the temperature gradient on the boundaries of a single cable.

We show the gradient control for one example where the number of single cables is $N = 7$ and $q = 3$. The explicit indication of the current loads and material parameters is renounced. Fig. 6 illustrates the necessary steps to compute the jumps in the Neumann data (cf. Fig. 6c) in COMSOL Multiphysics 3.5a. Apart from the calculation of the temperature profile (Fig. 6a) and the adjoint (Fig. 6b), we have to project the temperature distribution on the single cable core (Fig. 7a), its complement (Fig. 7b), the single cable insulation (Fig. 8a) and also its complement onto separate domains (Fig. 8b). This is required because if we compute the temperature distribution in COMSOL and the difference of the derivatives to the outer and inner normal directly, we obtain completely wrong results. It is due to an internal smoothing of the function in COMSOL. To deal with the problem, the derivative to the outer normal is computed on the projected temperature on the domains (single cable core respectively insulation) and to the inner normal on their complements. Finally, this procedure yields correct gradients and has to be performed for every single cable.

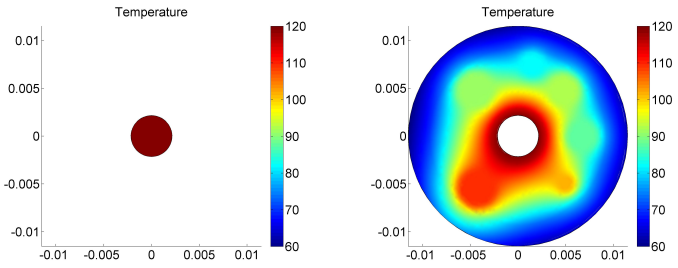

(a) (b)

Fig. 7: Temperature distribution on (a) a single cable core and (b) on its complement.

The partial derivatives obtained in this specific example, computed via the adjoint method, are:

$$\frac{\partial J}{\partial \Omega(\tilde{x_1})} \approx -498.2 \quad \frac{\partial J}{\partial \Omega(\tilde{y_1})} \approx -2123 \quad \frac{\partial J}{\partial \Omega(\tilde{x_2})} \approx 1660 \quad \frac{\partial J}{\partial \Omega(\tilde{y_2})} \approx -1668$$

$$\frac{\partial J}{\partial \Omega(\tilde{x_3})} \approx 5088 \quad \frac{\partial J}{\partial \Omega(\tilde{y_3})} \approx 6291 \quad \frac{\partial J}{\partial \Omega(\tilde{x_4})} \approx -181.4 \quad \frac{\partial J}{\partial \Omega(\tilde{y_4})} \approx -1070$$

$$\frac{\partial J}{\partial \Omega(\tilde{x_5})} \approx -2334 \quad \frac{\partial J}{\partial \Omega(\tilde{y_5})} \approx 2245 \quad \frac{\partial J}{\partial \Omega(\tilde{x_6})} \approx -1650 \quad \frac{\partial J}{\partial \Omega(\tilde{y_6})} \approx -1844$$

$$\frac{\partial J}{\partial \Omega(\tilde{x_7})} \approx -911.9 \quad \frac{\partial J}{\partial \Omega(\tilde{y_7})} \approx 169.2$$

In Table 1, h denotes a measure for the mesh refinement on the entire multicable domain, hnumedg for the refinement on the edges. Smaller values

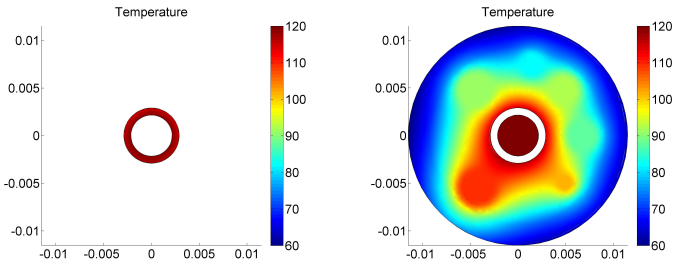

(a) (b)

Fig. 8: Temperature distribution on (a) a single cable insulation and (b) on its complement.

for h and higher values for hnumedg [2] result in finer grids and higher numbers of degrees of freedom (DOF). The maximum absolute discrepancy between adjoint and finite differences method $\max(\mathrm{err}_{\mathrm{abs}})$ is obtained in the partial derivative to the component Comp. The maximum relative error $\max(\mathrm{err}_{\mathrm{rel}})$ does not have to occur in the same component. It represents the maximum of discrepancy divided by the derivative value obtained via finite differences in all components. The quantities t_{ADJ} and t_{FD} specify the time in seconds necessary for the gradient determination with each method, Δt their difference in time.

h (hnumedg)	DOF	$\max(\mathrm{err}_{\mathrm{abs}})$ [Comp]	$\max(\mathrm{err}_{\mathrm{rel}})$	$t_{\mathrm{ADJ}}[s]$	$t_{\mathrm{FD}}[s]$	$\Delta t[s]$
5 (10)	26002	6.712 $[x_5]$	1.06e-2	25.8	560.4	534.6
5 (20)	70842	2.050 $[y_4]$	3.75e-3	44.7	1059.1	1024.2
4 (30)	148730	1.332 $[y_4]$	1.25e-3	98.9	2704.2	2605.3

Table 1: Statistics concerning mesh refinement, degrees of freedom, absolute resp. relative discrepancies between adjoint and non-adjoint method and calculation times for the specific example with seven single cables.

We state a good accordance of the gradients calculated via the adjoint method and finite differences with $\epsilon = 1.0\text{e-}4$, especially for higher numbers of degrees of freedom. Thus, to have a reliable gradient approximation, we have to use fine meshes. Furthermore, the computation times by the adjoint method are much shorter than those of the finite difference method. We have to admit that the second, neither the method itself, nor the implementation, is optimized. Nevertheless, it is obvious that the adjoint method works much faster in this scope because, additional to the one solution of the state system, the adjoint system, which is only semilinear, has to be solved once, independent

[2] The measure of refinement is a convention used in COMSOL Multiphysics 3.5a.

of the number of single cables. In contrast, the nonlinear state system must be solved twice for each optimization variable with finite differences (once if we used forward or backward instead of central differences) which corresponds to solving the partial differential equation 28 times in this example.

5.3 Computational algorithm

The implementation of the algorithm was performed in Matlab where the entire optimization procedure is guided (cf. Fig 9). First, geometrical and physical parameters are read from input files and convergence criteria of the algorithm, if necessary of the shape optimization procedure and the genetic algorithm, are defined. Depending on the multicable filling factor f and the number of single cables N, different strategies are proposed.

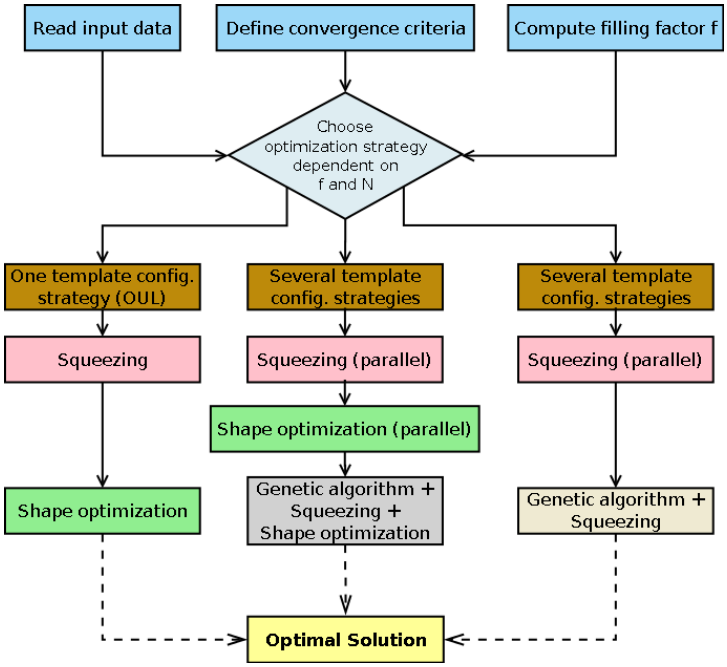

Fig. 9: Program flowchart of the entire multicable optimization procedure.

In case of low numbers of N and enough space in the multicable, we use only one initial template configuration. By experience, we recommend OUL. After the squeezing algorithm (implemented in Matlab), one shape optimization procedure in IPOPT is performed (cf. Fig. 10), yielding the (approximately) best solution.

For cables that are packed very densely (filling factors higher than 90%), shape optimization does not make sense. Instead, we apply the presented initial template configurations to produce initial multicable configurations by running the squeezing algorithm in parallel. They are given to the genetic algorithm where new configurations are produced and made feasible by squeezing. This procedure, realized in Matlab, takes extremely long and in some cases, it does not provide a better solution than the best inital configuration.

Moderately packed multicables which are common in practice require a quite complex procedure. Initial configurations, generated by the proposed heuristics for template configurations, by application of the squeezing algorithm and shape optimization, are passed on to the genetic algorithm. Therein, new configurations and finally the approximated global minimum are created by means of squeezing and shape optimization. The initial configurations, but also several ones during the genetic optimization, are evaluated in parallel in order to save time.

One shape optimization procedure consists of solving the state system (2) and the adjoint system (10) which is implemented in COMSOL Multiphysics 3.5a, controled via a Matlab script. Therein, an automatic mesh generator is applied as well as a damped Newton method [7] to solve the nonlinear partial differential equation. In every Newton step, we use UMFPACK [8,9] or PARDISO [25,**?**] for the solution of the linearized systems. For further details, we refer to [5,11].

Moreover, the shape gradient (13) is determined as described in section 5.2. Shape gradient, solution of state respectively adjoint system, the optimization constraints defined in $\mathcal{O}_{\mathrm{ad}}$, the constraints' derivatives and an initial multicable configuration are given to IPOPT which then computes a local minimum (cf. Fig. 10).

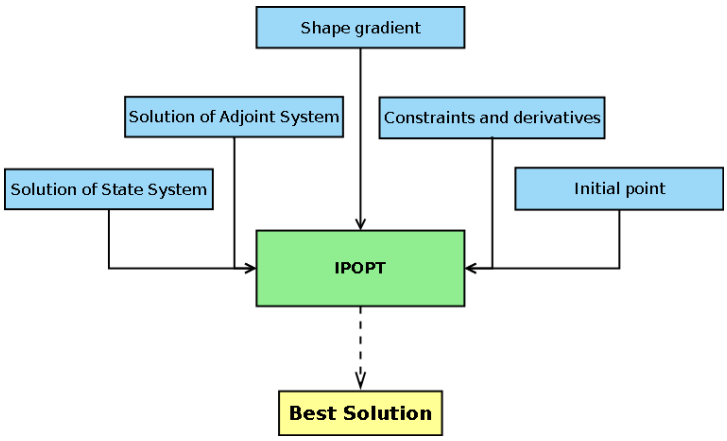

Fig. 10: Program flowchart of the shape optimization procedure.

IPOPT is a software package for large-scale nonlinear optimization that implements an interior-point line-search filter method (cf. [30,**?**,32]). In our options, we use a monotone strategy for the barrier parameter μ of the logarithmic barrier function. If this barrier parameter is small enough and the KKT conditions are fulfilled satisfactorily, an optimum is reached. Else, if after a given number of iterations $n_{\max}$ no minimum is attained, the procedure is interrupted automatically.

6 Numerical results

To test our proposed algorithms, we optimize the shape of different multicables, consisting of 1, 3, 15 and 33 single cables. In case of 1 and 3 single cables, the first strategy, consisting of exclusive application of shape optimization, is sufficient. In case of 15 and 33, we use the second strategy.

6.1 First example

We first optimize the position of only one single cable in the multicable with solid insulation material of lower heat conductivity inside and the exterior insulation of PVC. This single cable carries a current of $I_1 = 102\,\mathrm{A}$ and its cross sectional area is $A_1 \approx 14.5\,\mathrm{mm}^2$. We suppose the ambient temperature to be $33.2\,^\circ\mathrm{C}$. For the shape functional, we set $q = 2$.

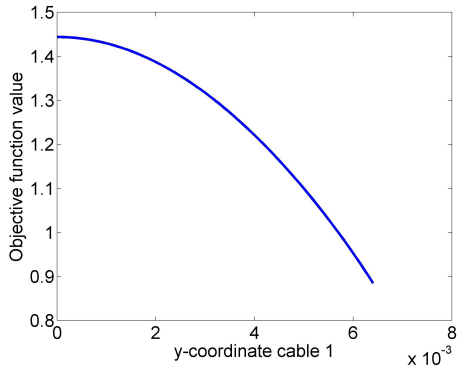

Fig. 11: Objective function values for variation of the y-coordinate of one single cable.

As the x-coordinate of the midpoint of the first single cable is fixed to zero and the y-coordinate ≥ 0, the objective function value is monotonically decreasing for single cable y-positions of the first cable (cf. Fig. 11). The highest value is obtained at the origin of the coordinate system ($J \approx 1.4439$), the

lowest at the exterior boundary ($J \approx 0.8866$). Table 2 shows the optimization progress in IPOPT where $\Delta\mathbf{x}$ denotes the Euclidean norm of the step size for the optimization variable in each optimization iteration. F-count indicates the number of function evaluations from one iteration to the next. The computation time was about 328 s with $\approx$ 45000 degrees of freedom in the linear system of every Newton iteration.

Iter	F-count	$J(\Omega)$	$\Delta\mathbf{x}$
0	1	1.4438692	
1	1	0.8963279	3.93e-2
2	1	1.2103676	8.38e-3
3	1	1.0596074	1.20e-3
4	1	0.9627317	7.63e-4
⋮	⋮	⋮	⋮
9	4	0.8868828	1.17e-5
10	4	0.8868126	1.03e-5
11	1	0.8865531	1.45e-7

Table 2: Optimization progress for a multicable with one single cable.

Obviously, the optimization works very well. During the optimization process, the single cable, starting from the origin of the coordinate system (Fig. 12a), runs out to the exterior boundary (Fig. 12c). Fig. 12 depicts the temperature distribution for three different configurations, each generated during the optimization process.

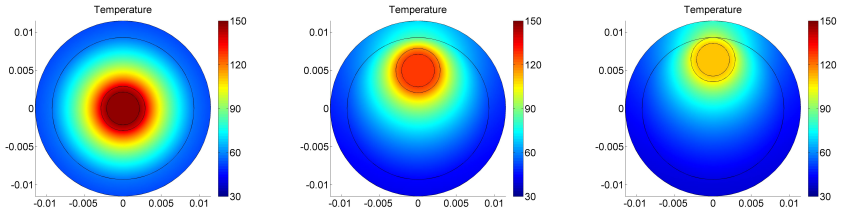

(a) (b) (c)

Fig. 12: Cable configurations generated during the optimization process: (a) Inital configuration with $J(\Omega) = 1.44387$, (b) configuration in iteration 3 with $J(\Omega) = 1.0596074$, and (c) final configuration with $J(\Omega) = 0.88655$.

Although with $q = 2$, $J(\Omega)$ does not approximate the $L^\infty(\Omega)$-norm very accurately, the maximum temperature is with $\approx$ 111.8 °C in the optimized multicable much lower than at the initial configuration ($\approx$ 147.9 °C). The reason is that if the single cable is nearer to the exterior boundary, more heat

is emitted to the environment by convection and radiation than it is the case if the hotspot is situated in the centre of the multicable.

6.2 Second example

6.2.1 Multicable consisting of three single cables of equal current loads

In our second example, we investigate a multicable consisting of three single cables with equal currents $I_1 = I_2 = I_3 = 89\,\mathrm{A}$ and cross sectional areas $A_1 = A_2 = A_3 = 14.5\,\mathrm{mm}^2$. We set $q = 3$.

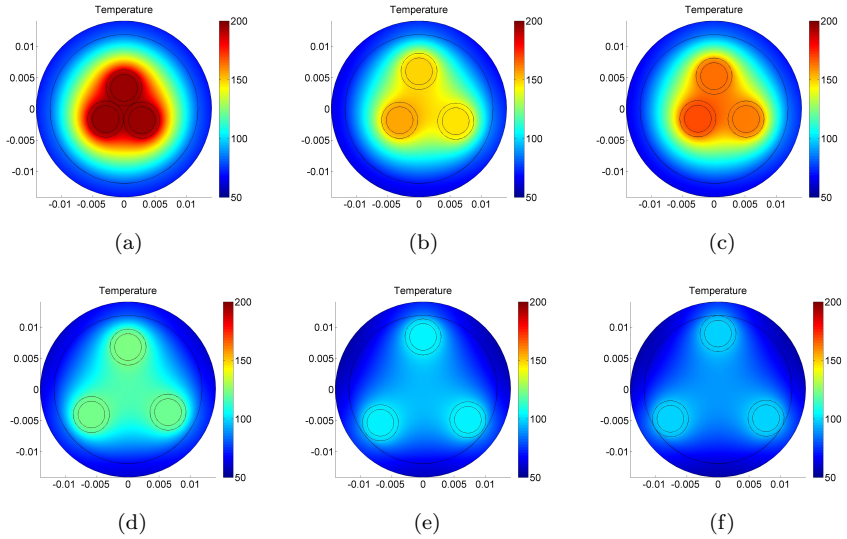

Fig. 13: Cable configurations generated during the optimization process for a multicable which consists of three single cables carrying equal current loads: (a) Initial configuration, (b) configuration in iteration 1, (c) configuration in iteration 2, (d) configuration in iteration 5, (e) configuration in iteration 9, and (f) configuration in iteration 30.

Starting with an almost regular positioning such that the midpoints of the single cables nearly form an equilateral triangle (cf. Fig. 13a), the single cables run out to the boundary again. Having reached the boundary, they are forced to find a configuration where the cables have the largest possible distance from each other, i. e. an equilateral triangle of the midpoints with each single cable situated at the boundary of the multicable (cf. Fig. 13f).

In IPOPT, it sometimes happens that the objective function value increases in an iteration e. g. in our case at the second iteration (cf. Table 3 and Fig.

Iter	F-count	$J(\Omega)$	$\Delta\mathbf{x}$
0	1	5.0743619e+02	
1	2	3.0311155e+02	5.32e-01
2	1	3.6448495e+02	9.96e-03
3	1	2.0319573e+02	3.25e-03
4	1	2.1952290e+02	3.87e-04
5	1	1.9638202e+02	4.28e-04
⋮	⋮	⋮	⋮
8	1	1.3197190e+02	5.74e-05
9	1	1.3202247e+02	4.14e-05
10	1	1.2003736e+02	4.30e-04
⋮	⋮	⋮	⋮
28	11	1.1789933e+02	2.84e-04
29	13	1.1789923e+02	2.97e-04
30	14	1.1789918e+02	2.98e-04

Table 3: Optimization progress first example.

14). This is due to the interior-point algorithm when the barrier parameter is modified [30]. The entire optimization is interrupted after thirty iterations, that is $n_{\max} = 30$.

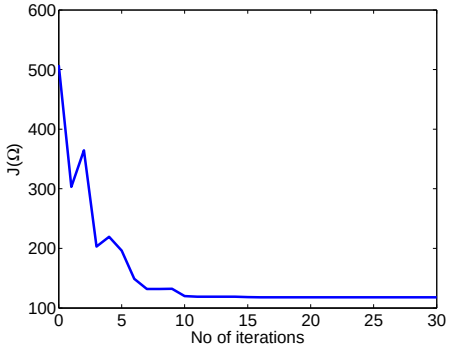

Fig. 14: Convergence history of the optimizer for three single cables.

Obviously, the maximum temperature decreases from $\approx 197\,^{\circ}\mathrm{C}$ to $\approx 100\,^{\circ}\mathrm{C}$ during the optimization process (cf. Table 4). The reason is again that more thermal energy can be emitted at the transition to air if the single cables are placed at the exterior boundary. At the final configuration, they have the greatest possible distances from each other.

The insulation material of the single cables and the exterior insulation is supposed to consist of PVC, again. Assumed a melting point of about $130\,^{\circ}\mathrm{C}$, the initial multicable would not be able to endure the given current loads whereas the optimized one could without any problems.

Statistics			
Init $\max_{\mathbf{x}\in\Omega} T(\mathbf{x})$	196.5 °C	Final $\max_{\mathbf{x}\in\Omega} T(\mathbf{x})$	99.7 °C
No of iterations	30	No of function evaluations	63
Time optimizer	≈ 42 s	Time FEM solver	≈ 3584 s
Time squeezing	≈ 1.1 s	Total time	≈ 3632 s
DOFs	≈ 120000	NOEs	≈ 30000

Table 4: Statistics for optimization with three single cables.

The inner insulation heat conductivity is computed according to the given formula in [11]. Thus, it is supposed to be a mixture of air and solid material. The modelling of inner heat conductivity with such low filling factors ($f \leq 30\,\%$) might be inadequate. If we assume the inner material to consist entirely of solid material, e. g. PVC ($\lambda^{\text{gaps}} = 0.19\,\text{W}/(\text{m}\cdot\text{K})$), the maximum temperature decreases by shape optimization from 102.1 °C to 92.0 °C.

Concerning the calculation expense, most of the time is spent to solve state and adjoint systems during the 63 iterations (cf. Table 4 with further statistical information). The squeezing time is nearly negligible and computation time in the optimizer is very low. In fact, the optimization problem to be solved in the nonlinear optimizer is very small. Neglecting the x-coordinate of the first single cable as well as the lower and upper bounds for the other variables, it consists of 5 optimization variables and 6 geometrical constraints. For higher values of q, it is even more expensive to solve the PDEs. With $q = 5$, we obtained nearly the same optimization process (with of course higher values for $J(\Omega)$) and similar computation times in the optimizer, but the solution of the PDEs took about four times longer at equal mesh refinements.

6.2.2 Multicable consisting of three single cables of different current loads

We suppose again $N = 3$, $q = 3$, equal cross sectional areas for the single cables and the same material and ambient parameters as in the previous example. The only difference is that now the cables carry different current loads, namely $I_1 = 103\,\text{A}$ and $I_2 = I_3 = 80\,\text{A}$.

Starting from the same initial configuration as in subsection 6.2.1, the cables run out to the exterior border, again (cf. Fig. 15). In contrast, they move until finally the centre coordinates form an isosceles triangle which is not equilateral (cf. Fig. 15f). The distance to the single cable carrying higher current is larger than between the cables with equal currents. The objective function value for $q = 3$ improves from $J(\Omega_{\text{init}}) \approx 486.3$ to $J(\Omega_{\text{opt}}) \approx 118.3$ and the maximum temperature decreases from $\max_{\mathbf{x}\in\Omega_{\text{init}}} T(\mathbf{x}) \approx 199.2\,°\text{C}$ to $\max_{\mathbf{x}\in\Omega_{\text{opt}}} T(\mathbf{x}) \approx 115.3\,°\text{C}$.

The entire optimization took 4991 seconds with 30 optimization steps and 84 function evaluations. 42 seconds where needed in the nonlinear optimizer, one second for squeezing, the rest to solve the PDEs. The number of elements

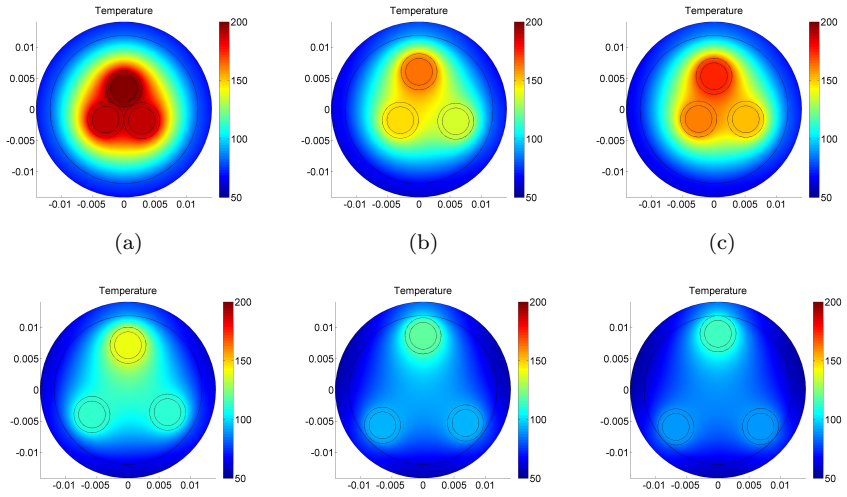

Fig. 15: Cable configurations generated during the optimization process for a multicable consisting of three single cables carrying different current loads: (a) Initial configuration, (b) configuration in iteration 1, (c) configuration in iteration 2, (d) configuration in iteration 5, (e) configuration in iteration 10, and (f) configuration in iteration 30.

was about 30000, corresponding to $\approx$ 120000 degrees of freedom in the linearized systems which were solved by UMFPACK.

6.3 Third example

We consider a multicable consisting of 15 single cables with different cross sectional areas and currents as listed in Table 5. The filling factor of the multicable is $f \approx 47\,\%$, the ambient temperature $T^{\mathrm{amb}} = 33.2\,^{\circ}\mathrm{C}$ and we use $q = 3$, again. The maximum temperatures of the depicted initial configurations, which were obtained by squeezing of the initial template configurations (cf. Fig. 16), are between $142.2 - 149.7\,^{\circ}\mathrm{C}$.

The lowest maximum temperature after shape optimization applied to the initial template configurations, thus the maximum of the best individual for the initial generation, is $127\,^{\circ}\mathrm{C}$. After a total computation time of nearly 30 h with about 7100 function evaluations[3], partly in parallel, we obtain our approximated global minimal maximum temperature.

Therein, each shape optimization in IPOPT was interrupted after no later than 30 iterations. In each function evaluation, $30000 - 40000$ elements with

[3] Each function evaluation includes the solution of state and adjoint system.

Single Cable No.	I_k (A)	A_k (mm^2)	J_k (A/mm^2)
1	53.00	14.5	3.65
2	82.00	8.30	9.89
3	12.00	8.30	1.45
4	12.00	3.46	3.46
5	52.00	8.30	6.27
6	43.00	5.73	7.51
7	14.88	5.73	2.60
8	16.20	5.73	2.83
9	18.00	3.46	5.20
10	18.00	3.46	5.20
11	9.50	1.33	7.16
12	9.50	1.33	7.16
13	10.00	0.68	14.72
14	4.50	0.68	6.62
15	0.34	0.50	0.68

Table 5: Currents and cross sectional areas of the metallic core for the multicable consisting of 15 single cables.

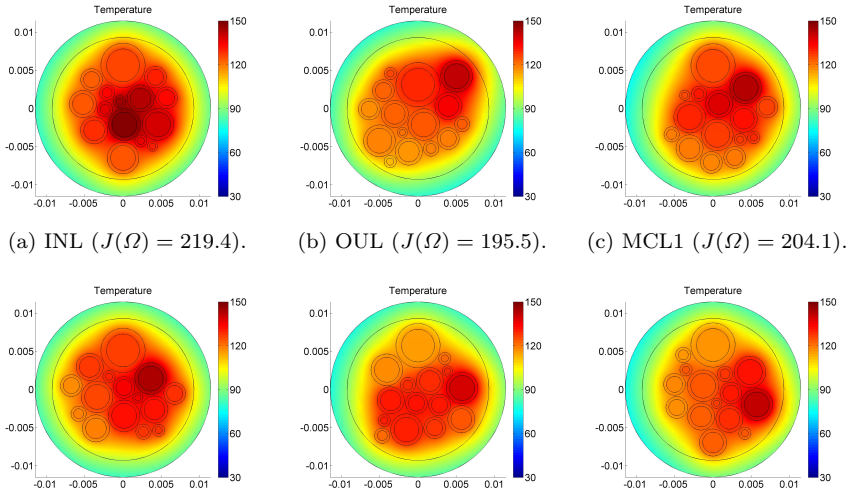

(a) INL ($J(\Omega) = 219.4$). (b) OUL ($J(\Omega) = 195.5$). (c) MCL1 ($J(\Omega) = 204.1$).

(d) OUL2 ($J(\Omega) = 207.2$). (e) OUL4 ($J(\Omega) = 198.0$). (f) OPP ($J(\Omega) = 193.8$).

Fig. 16: Temperature distributions in multicables consisting of 15 single cables for different initial template assignments.

$120000 - 160000$ degrees of freedom were used for the finite element approximation. The linear solver was UMFPACK. The entire optimization problem had 29 optimization variables (x-coordinate of first single cable neglected) with 120 inequality constraints and 435 non-zero entries in the inequality constraint Jacobian.

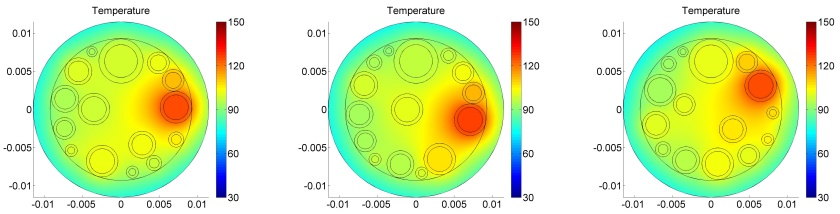

(a) (b) (c)

Fig. 17: Improved cable configurations obtained by application of the genetic algorithm for 15 single cables: (a) Best GA configuration with $J(\Omega) = 134.9$, (b) second GA configuration with $J(\Omega) = 135.0$, and (c) third GA configuration with $J(\Omega) = 137.0$.

Generation	Individual No.								
No.	1	2	3	4	5	6	7	8	9
0	154.0	136.7	137.7	139.8	147.0	141.0	157.5	136.5	140.7
1	136.5	143.6	140.3	141.5	147.9	142.8	142.4	136.2	143.1
2	136.2	141.7	142.3	147.8	140.3	142.0	137.0	142.3	142.8
3	136.2	135.8	137.6	142.6	135.8	150.8	147.8	144.2	149.6
4	135.8	134.9	138.8	140.6	138.8	140.1	146.4	146.1	137.3
5	134.9	137.0	141.8	135.0	146.6	141.7	140.4	143.4	140.2

Table 6: Fitness values of all individuals for 5 generations in the progress of the genetic algorithm for 15 single cables.

The minimal maximum temperature of our best cable configuration is 125.9 °C. Hence, in this case with a rather low filling factor, most of the optimization is done by the gradient-based shape optimization. The influence of the genetic algorithm is rather small in relation to the computation effort (see also Fig. 18a and Table 6). But this also shows that the different template configuration strategies, combined with squeezing and shape optimization, already provide a good approximation of the best cable configuration.

6.4 Fourth example

Finally, we optimize the multicable that presented the motivation for our paper. It consists of 33 single cables. We drop the explicit specification of all current loads and cross sectional areas. Fig. 19 depicts the current load over cross sectional area for each single cable. Furthermore, we use $T^{\text{amb}} = 33.2\,^{\circ}\text{C}$ and $q = 2$. The filling factor of the multicable is $f \approx 63\,\%$ with an inner diameter of 19.2 mm and outer diameter of 23.6 mm for the exterior insulation.

Fig. 20 shows that the maximum temperature obtained by the initial template configuration INL (Fig. 20a) is 108.5 °C. In contrast, our optimized cable

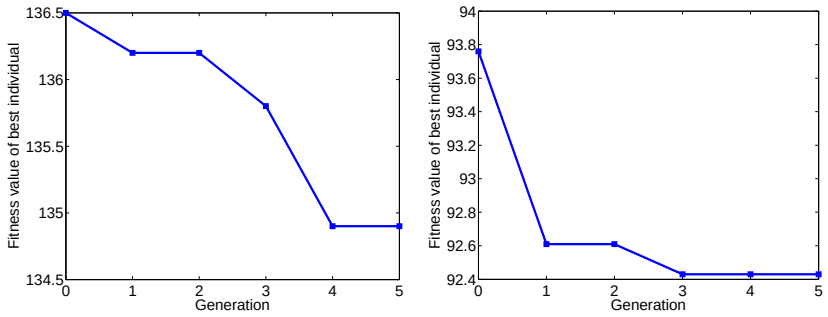

(a) (b)

Fig. 18: Convergence history of genetic algorithm for (a) 15 single cables and (b) 33 single cables.

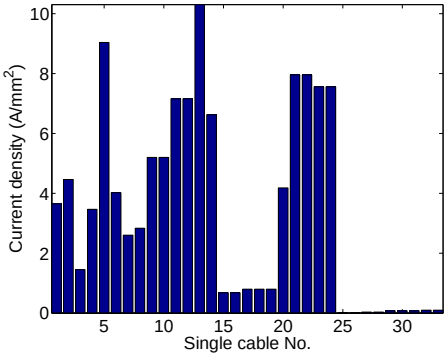

Fig. 19: Current densities of the 33 single cables in the multicable.

has a maximum temperature of 92.4 °C (Fig. 21a). That means that the difference in maximum temperatures between a bad and good configuration for this case can be about 16.1 °C. Thus, less ambient temperature, the reduction of maximum temperature of the optimized cable compared to that obtained with INL is $\approx 21\,\%$.

For the optimization via the genetic algorithm, 5 generations with each consisting of 9 individuals where determined (cf. Table 7). Therein, the objective function value was reduced from $J(\Omega_{\text{init}}) = 93.76$ to $J(\Omega_{\text{opt}}) = 92.43$ (cf. Fig. 18b). The shape optimization of each individual in IPOPT was interrupted after latest $n_{\max} = 50$. The number of optimization variables was 65 with 561 inequality constraints and 2145 non-zero entries in the inequality constraint Jacobian. The linearized systems in the evaluation with finite elements were solved with PARDISO and had between 250000–350000 unknowns.

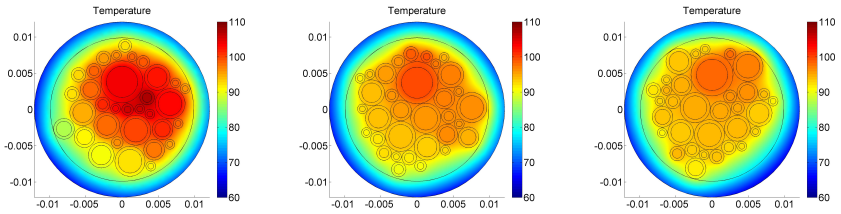

(a) INL ($J(\Omega) = 116.2$). (b) OUL ($J(\Omega) = 108.3$). (c) OPP ($J(\Omega) = 106.1$).

Fig. 20: Temperature distributions in multicables consisting of 33 single cables for different initial template assignments.

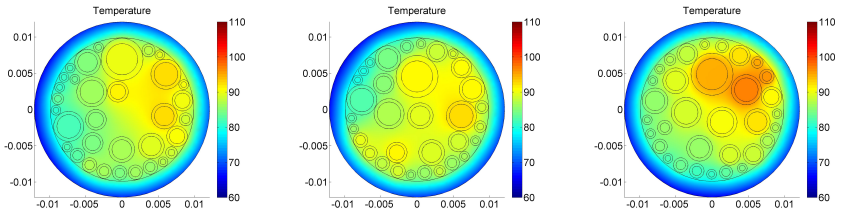

(a) (b) (c)

Fig. 21: Improved cable configurations obtained by application of the genetic algorithm for 15 single cables: (a) Best GA configuration with $J(\Omega) = 92.43$, (b) second GA configuration with $J(\Omega) = 93.81$, and (c) third GA configuration with $J(\Omega) = 96.89$.

Generation	Individual No.								
No.	1	2	3	4	5	6	7	8	9
0	99.05	96.59	99.64	96.48	97.53	96.76	95.81	97.37	93.76
1	93.76	95.39	96.30	99.12	93.09	95.68	92.61	95.13	98.45
2	92.61	99.65	98.34	94.54	96.37	97.87	97.88	97.33	98.70
3	92.61	96.90	97.92	92.43	96.00	95.86	94.92	95.04	98.16
4	92.43	95.97	95.50	95.75	96.59	96.09	99.61	96.75	95.79
5	92.43	98.18	98.11	93.81	97.45	99.12	98.65	97.04	96.89

Table 7: Fitness values of all individuals for 5 generations in the progress of the genetic algorithm for 33 single cables.

Altogether, the state and adjoint systems were evaluated about 7300 times. The entire optimization process took about 42 hours.

7 Conclusion

The goal of this paper was to derive an algorithm for the optimization of current carrying multicables. This was enabled by coupling a cable squeezing algorithm, helping to find feasible cable configurations, to a genetic algorithm and a gradient-based shape optimization approach. Surprising in this context is the positive influence of the gradient-based shape optimization for multicables consisting of several single cables. In advance, we expected it to fail there as with little available space, the shape could hardly be influenced. In fact, this gradient based approach runs into local minima which are numerous for higher numbers of single cables. In combination with the genetic algorithm, the global optimum is however approximated in acceptable time, running several instances in parallel.

We showed how a well thought-out and precise cable production process could improve the thermal on-board management in cars just by varying cable positions. This fact has not or hardly been paid attention to. By now, the production process for multicables and cable harnesses is not as precise as necessary for an optimal design. Nevertheless, it is already helpful for the manufacturers to have the knowledge about an optimized cable design.

Our algorithm is also interesting for high voltage wiring-harnesses of hybrid and electric vehicles [17] with cables which consist of lower numbers of single cables. Practical applications in vehicles require electrical cables which contain from one and up to five electrically insulated conductors. In these cases, the pure application of shape optimization is sufficient as demonstrated in the numerical examples.

Within this paper, we supposed the multicables to be suspended in free air and to have rather low ambient temperatures. For that the cables always run out to the exterior border if possible. Supposing, for example, different temperatures at the upper and lower side could be integrated simply. It would influence the optimization procedure and in consequence the optimal cable design.

It is intended to extend the approach to the thermal optimization of current distribution boxes consisting of several components. The number of degrees of freedom of the components geometries represents a real challenge for future work.

Acknowledgments

The authors thank Thomas Apel, Benjamin Nolet and Max Winkler for their help in the implementation of the algorithms, for valuable hints concerning the problem definition and the optimization strategy and for proofreading of the article.

References

1. S.W. Churchill, R. Usagi. *A general expression for the correlation of rates of transfer and other phenomena.* AIChE J. **18**(6) (1972), 1121–1128.
2. Ra. Ciegis, Re. Ciegis, M. Meilunas, G. Jankeviciute, V. Starikovtius. *Parallel numerical algorithms for optimization of electrical cables.* Math. Model. Anal. **13**(4) (2008), 471–482.
3. R. Ciegis, A. Ilgevicius, G. Jankeviciute, M. Meilunas. *Determination of heat conductivity coefficient of a cable bundle by inverse problem solution method.* Electron. Electr. Eng. **2** (2009), 77–80.
4. R. Ciegis, A. Ilgevicius, H.-D. Liess, M. Meilunas, O. Suboc. *Numerical simulation of the heat conduction in electrical cables.* Math. Model. Anal. **12** (2007), 425–439.
5. COMSOL Multiphysics. *Reference guide version 3.5a.* 2008.
6. M. Delfour, J.-P. Zolesio. *Shapes and geometries.* SIAM, Philadelphia, 2011.
7. P. Deuflhard. *A modified Newton method for the solution of ill-conditioned systems of nonlinear equations with application to multiple shooting.* Numer. Math. **22** (1974), 289–315.
8. T.A. Davis. *Algorithm 832: UMFPACK, an unsymmetric-pattern multifrontal method.* ACM Transactions on Mathematical Software **30**(2) (2004), 196–199.
9. T.A. Davis and I.S. Duff. *An unsymmetric-pattern multifrontal method for sparse LU factorization.* SIAM Journal on Matrix Analysis and Applications **18**(1) (1997), 140–158.
10. K. Dvorsky. *Analysis of a nonlinear boundary value problem with application to heat transfer in electric cables.* Ph.D. dissertation, Fac. Aerosp. Tech., Univ. German Federal Armed Forces, Munich, 2012.
11. K. Dvorsky, H.-D. Liess, F. Loos, *Two approaches for heat transfer simulation of current carrying multicables.* Preprint, MATCOM-D-12-00205, 2012.
12. H. Harbrecht. *On analytical derivatives for geometry optimization in the polarizable continuum model.* J. Math. Chem. **49**(9) (2011), 1928–1936.
13. H. Harbrecht, J. Tausch. *An efficient numerical method for a shape-identification problem arising from the heat equation.* Inverse Problems **27** (2011), 065013.
14. R. Haupt, S. Haupt. *Practical genetic algorithms.* 2nd edition, John Wiley & Sons, New York, NY, USA, 1998.
15. F. Hettlich, W. Rundell. *The determination of a discontinuity in a conductivity from a single boundary measurement.* Inverse Problems **14** (1998), 67–82.
16. F. Hettlich, W. Rundell. *Identification of a discontinuous source in the heat equation.* Inverse Problems **17** (2001), 1465–1482.
17. C. Holyk, H.-D. Liess, S. Grondel, H. Kanbach, F. Loos. *Simulation and measurement of the stationary temperature in multi-conductor cables for hybrid and electric vehicles.* Submitted to Electr Pow Syst Res, Elsevier, 2013.
18. S.Y. Huang, F. Mayinger. *Wärmeübergang bei freier Konvektion um elliptische Rohre.* Wärme- und Stoffübertragung **18**(3) (1984), 175–183.
19. A. Ilgevicius. *Analytical and numerical analysis and simulation of heat transfer in electrical conductors and fuses.* Ph.D. dissertation, Fac. Elec. Inform. Tech., Univ. German Federal Armed Forces, Munich, 2004.
20. H. Kasumba, K. Kunisch. *On free surface PDE constrained shape optimization problems.* Appl. Math. Comput. **218**(23) (2012), 11429–11450.
21. MathWorks. *Using the genetic algorithm: user's guide (R2010b).* Retrieved February 26, 2013 from www.mathworks.com/help/gads.
22. J. Murat, J. Simon. *Étude de problémes d'optimal design* in Optimization Techniques, Modeling and Optimization in the Service of Man, edited by J. Céa, Lect. Notes Comput. Sci. **41**, Springer-Verlag, Berlin, 54–62, 1976.
23. O. Pironneau. *Optimal shape design for elliptic systems.* Springer, New York, 1983.
24. O. Pironneau, B. Mohammadi. *Applied shape optimization in fluids.* Oxford University Press Inc, New York, 2001.
25. O. Schenk and K. Gärtner. *Solving unsymmetric sparse systems of linear equations with PARDISO.* Journal of Future Generation Computer Systems **20**(3) (2004), 475–487.

26. O. Schenk and K. Gärtner. *On fast factorization pivoting methods for symmetric indefinite systems.* Elec. Trans. Numer. Anal. **23** (2006), 158–179.
27. S. Schmidt. *Efficient large scale aerodynamic design based on shape calculus.* Ph.D. dissertation, University of Trier, Germany, 2010.
28. J. Sokolowski, J.-P. Zolesio. *Introduction to shape optimization.* Springer, Berlin, 1992.
29. F. Tröltzsch. *Optimale Steuerung partieller Differentialgleichungen. Theorie, Verfahren und Anwendungen.* Vieweg, Wiesbaden, 2005.
30. A. Wächter. *Short tutorial: Getting started with IPOPT in 90 minutes.* In Combinatorial Scientific Computing, Dagstuhl Seminar Proceedings 09061, Schloss Dagstuhl – Leibniz-Zentrum für Informatik, Dagstuhl, Germany, 2009, http://drops.dagstuhl.de/opus/volltexte/2009/2089.
31. A. Wächter and L.T. Biegler. *Line search filter methods for nonlinear programming: Motivation and global convergence.* SIAM Journal on Optimization **16**(1) (2005), 1–31.
32. A. Wächter and L.T. Biegler. *On the implementation of a primal-dual interior point filter line search algorithm for large-scale nonlinear programming.* Mathematical Programming **106**(1) (2006), 25–57.

LATEST PREPRINTS

No.	Author: *Title*
2013-01	**H. Harbrecht, M. Peters** *Comparison of Fast Boundary Element Methods on Parametric Surfaces*
2013-02	**V. Bosser, A. Surroca** *Elliptic logarithms, diophantine approximation and the Birch and Swinnerton-Dyer conjecture*
2013-03	**A. Surroca Ortiz** *Unpublished Talk: On some conjectures on the Mordell-Weil and the Tate-Shafarevich groups of an abelian variety*
2013-04	**V. Bosser, A. Surroca** *Upper bound for the height of S-integral points on elliptic curves*
2013-05	**Jérémy Blanc, Jean-Philippe Furter, Pierre-Marie Poloni** *Extension of Automorphisms of Rational Smooth Affine Curves*
2013-06	**Rupert L. Frank, Enno Lenzmann, Luis Silvestre** *Uniqueness of Radial Solutions for the Fractional Laplacian*
2013-07	**Michael Griebel, Helmut Harbrecht** *On the convergence of the combination technique*
2013-08	**Gianluca Crippa, Carlotta Donadello, Laura V. Spinolo** *Initial-Boundary Value Problems for Continuity Equations with BV Coefficients*
2013-09	**Gianluca Crippa, Carlotta Donadello, Laura V. Spinolo** *A Note on the Initial-Boundary Value Problem for Continuity Equations with Rough Coefficients*
2013-10	**Gianluca Crippa** *Ordinary Differential Equations and Singular Integrals*
2013-11	**G. Crippa, M. C. Lopes Filho, E. Miot, H. J. Nussenzveig Lopes** *Flows of Vector Fields with Point Singularities and the Vortex-Wave System*
2013-12	**L. Graff, J. Fender, H. Harbrecht, M. Zimmermann** *Key Parameters in High-Dimensional Systems with Uncertainty*
2013-13	**Jérémy Blanc, Immanuel Stampfli** *Automorphisms of the Plane Preserving a Curve*

LATEST PREPRINTS

No. **Author:** *Title*

2013-14 **Jérémy Blanc, Jung Kyu Canci**
Moduli Spaces of Quadratic Rational Maps with a Marked Periodic Point of Small Order

2013-15 **Marcus J. Grote, Johannes Huber, Drosos Kourounis, Olaf Schenk**
Inexact Interior-Point Method for Pde-Constrained Nonlinear Optimization

2013-16 **Helmut Harbrecht, Florian Loos,**
Optimization of Current Carrying Multicables